Towards combined transport and optical studies of the 0.7-anomaly in a quantum point contact

Enrico Schubert[*,1], Jan Heyder[1,2], Florian Bauer[1,2], Wolfgang Stumpf[3], Werner Wegscheider[3], Jan von Delft[1,2], Stefan Ludwig[1], Alexander Högele[1]

[1] Center for NanoScience and Fakultät für Physik,
Ludwig-Maximilians-Universität München, Geschwister-Scholl-Platz 1, 80539 München, Germany
[2] Arnold Sommerfeld Center for Theoretical Physics,
Ludwig-Maximilians-Universität München, Theresienstrasse 37, 80333 München, Germany
[3] Laboratory for Solid State Physics, ETH Zürich, CH-8093 Zürich, Switzerland

Received XXXX, revised XXXX, accepted XXXX
Published online XXXX

Key words: Two-dimensional electron system, quantum point contact, 0.7-anomaly, optical spectroscopy.

[*] Corresponding author: e-mail enrico.schubert@physik.uni-muenchen.de, Phone: +49-89-2180-3349, Fax: +49-89-2180-3182

A Quantum Point Contact (QPC) causes a one-dimensional constriction on the spatial potential landscape of a two-dimensional electron system. By tuning the voltage applied on a QPC at low temperatures the resulting regular step-like electron conductance quantization can show an additional kink near pinch-off around $0.7e^2/h$, called 0.7-anomaly. In a recent publication, we presented a combination of theoretical calculations and transport measurements that lead to a detailed understanding of the microscopic origin of the 0.7-anomaly. Functional Renormalization Group-based calculations were performed exhibiting the 0.7-anomaly even when no symmetry-breaking external magnetic fields are involved. According to the calculations the electron spin susceptibility is enhanced within a QPC that is tuned in the region of the 0.7-anomaly. Moderate externally applied magnetic fields impose a corresponding enhancement in the spin magnetization. In principle, it should be possible to map out this spin distribution optically by means of the Faraday rotation technique. Here we report the initial steps of an experimental project aimed at realizing such measurements. Simulations were performed on a particularly pre-designed semiconductor heterostructure. Based on the simulation results a sample was built and its basic transport and optical properties were investigated. Finally, we introduce a sample gate design, suitable for combined transport and optical studies.

Copyright line will be provided by the publisher

arXiv:1403.8015v1 [cond-mat.mes-hall] 31 Mar 2014

1 Introduction A quantum point contact (QPC) is a short, 1-dimensional constriction usually realized within a 2-dimensional electron system (2DES), by applying voltage to metallic gates, thereby depleting the electrons beneath and only leaving a narrow transport channel whose width can be tuned by the applied gate-voltage. When a QPC is opened up by changing the applied gate-voltage, its conductance not only, famously, rises in integer steps of the conductance quantum, $G_Q = 2e^2/h$ [1,2,3], but also shows a shoulder-like intermediate step at the onset of the first plateau, around $\simeq 0.7G_Q$, that has a very intriguing dependence on temperature (T), magnetic field (B) and source-drain voltage (V_{SD}) [4,5,6,7]. This phenomenon is known as the 0.7-anomaly. A succinct summary of the status of various previous theoretical treatments thereof may be found in [8].

In a recent publication [9], we presented a combination of theoretical calculations and transport measurements that lead to a detailed understanding of the microscopic origin of the 0.7-anomaly. It is caused by a smeared van Hove peak in the local density of states (LDOS), whose weight, shape and position depends on sample geometry (width, length and shape of the QPC confinement potential). The peak enhances the effect of interaction by two main mech-

Copyright line will be provided by the publisher

anisms: first, it enhances the effective Hartree barrier, and thus the elastic back-scattering due to Coulomb repulsion; second, inelastic scattering is enhanced once phase space is opened up by increasing the temperature or the source-drain bias voltage.

The present paper serves two purposes. First, in section 2 we summarize some of the main results from [9], highlighting, in particular, one of its central predictions: the local spin susceptibility is predicted to be anomalously enhanced in the vicinity of the QPC. Second, in section 3 we describe the initial stages of an experimental project that ultimately aims at detecting the predicted anomalous behavior of the spin susceptibility in a QPC by optical methods.

2 Microscopic origin of the 0.7-anomaly We use a multi-gate sample that gives us direct control over the geometry of the confinement potential, defining the QPC. In this section we present both theoretical calculations and experimental measurements of transport of the lowest transverse mode, finding very good qualitative agreement for the conductance as a function of applied gate voltage at both zero and finite magnetic field. We predict the shapes of the spin-resolved conductance curves and show that

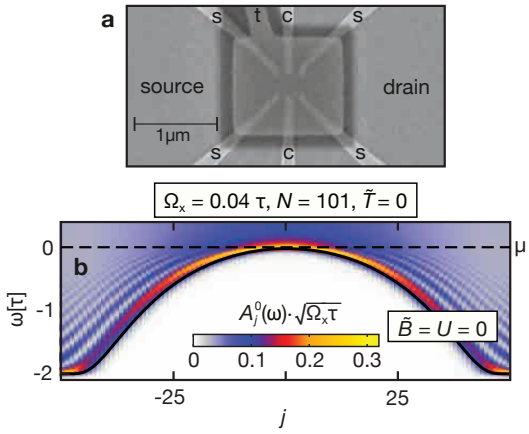

Figure 1 **a**, gate layout of one of our samples designed to investigate the 0.7-anomaly of QPCs. The metal gates (light gray) are placed with the help of electron-beam lithography on the surface of GaAs / AlGaAs heterostructures. The darker shaded areas consists of cross-linked PMMA which is used to electrically isolate vertically stacked metal gates. A semi-transparent titanium top-gate (gray, on top of PMMA) covers the nanostructure including its leads. Experiments were done at ultra-low temperatures (base temperature of 17 mK, electron temperature $T_0 \simeq$ 30 mK). **b**, the bare local density of states, $A_j^0(\omega)$, in the central region of the QPC as a function of site j and frequency ω. The maximum of A_j^0 follows the shape of the band, i.e. the shape of the applied potential, resulting in a distinct ridge-like structure (yellow), the van Hove ridge.

the 0.7-anomaly coming out of our calculations is directly linked to a smeared van Hove singularity, a maximum in the LDOS, located at the top of the 1D-potential which, in combination with interactions, gives rise to a strongly enhanced spin-susceptibility. We show that the strength of interaction within the constriction can be tuned by a global top-gate.

Our QPC design (see FIG.1**a**) allows a detailed tuning of the confinement potential within the 2DES both along and perpendicular to the electron propagation direction through the QPC, thereby defining the length and width of the QPC respectively . In addition to the two central gates (c) and four side gates (s), allowing for a fine-tuning of the effective 1D barrier, the sample also contains a global top-gate (t) to adjust the charge carrier density of the 2DES. The advantages of such a sample geometry are: first, in experiments it is often difficult to clearly distinguish the 0.7-anomaly from unwanted disorder related resonances, which can alter the results in an uncontrolled way. In our case the enhanced tunability via multiple control gates facilitates an unambiguous identification of the 0.7-anomaly and a sufficient separation from disorder induced resonances. This is extremely important for a quantitative comparison with model calculations, which assume a potential landscape without disorder. Second, the multi-gate structure enables us to monitor the evolution of the QPC properties with varying length and width independently, which makes it a versatile tool for a systematic analysis of the 0.7-structure.

The experimental realization of a QPC is modeled by a simple potential barrier describing the effective 1D-potential along the electronic transport direction. Information about the transverse structure of the channel is fully incorporated into a space-dependent model parameter U, defining the strength of interactions. After discretizing space the model Hamiltonian is given by

$$\hat{H} = \sum_{j\sigma} \left[E_{j\sigma} \hat{n}_{j\sigma} - \tau_j (d^\dagger_{j+1\,\sigma} d_{j\sigma} + \text{h.c.}) \right] + \\ + \sum_j U_j \hat{n}_{j\uparrow} \hat{n}_{j\downarrow} \,. \tag{1}$$

It describes an infinite tight-binding chain with nearest-neighbor hopping τ_j, on-site interactions U_j, and a uniform magnetic field, $\tilde{B} = g\mu_B B$, acting only to Zeeman-split opposite spins. (we use symbols with or without tildes, e. g. $\tilde{B}$ or B, to distinguish model parameters from experimental ones, respectively). Orbital effects are neglected, a good approximation if the field is parallel to the two-dimensional electron system). The on-site energy, $E_{j,\sigma} = E_j - \frac{\sigma}{2}\tilde{B}$, in combination with the hopping, τ_j, both vary smoothly with j, thus creating an effective potential barrier $V_j = E_j - (\tau_j + \tau_{j+1}) - \mu$, measured w.r.t. the chemical potential, μ (we use $\mu = 0$). We choose $U_j \neq 0$ and

Copyright line will be provided by the publisher

$E_j \neq 0$ only for N sites, symmetric around $j = 0$ that define the extent of the QPC. U_j is constant in the center of the QPC with $U_0 = U$ and drops smoothly to zero for $|j| \to N/2$. We choose the potential, V_j, to be symmetric and parabolic near the top, $V_j = \tilde{V}_c - \Omega_x^2/(4\tau_0)j^2$ with barrier-height $\tilde{V}_c$, mimicking the role of gate voltage from experiment, and curvature Ω_x, defining the effective length of the QPC (see supplementary information of [9] for more details). FIG.1**b** shows the bare LDOS, $A_j^0(\omega)$, of the QPC as a function of site j and frequency ω. The LDOS has a maximum right above the band bottom, visible as a yellow-red structure, that follows the shape of the potential (black thick line). This structure, which lies at the heart of the explanation for the 0.7-anomaly, will be called a "van Hove ridge". The ridge maximum lies slightly higher in energy than the potential V_j, by an amount that scales like the potential curvature Ω_x, where the LDOS is proportional to $1/\sqrt{\Omega_x \tau_0}$.

To investigate the influence of interactions we use the functional Renormalization Group (fRG)[10,11,12,13]. The fRG approach in essence corresponds to an RG-enhanced perturbation theory in U times the local density of states at the chemical potential. All results were obtained for zero temperature, $T = 0$. The calculation was done in Matsubara-space, uses the coupled-ladder approximation of the 2-particle vertex in both real-, and frequency-space and is exact to second order in the interaction (see supplement of [9]).

Fig. 2a / Fig. 2c show the calculated/measured $\tilde{V}_c$-dependence of the linear conductance $g = G/G_Q$ of the lowest mode of a QPC for several values of magnetic field and a finite interaction strength. We find very good qualitative agreement not only for zero field, where the asymmetry of the step becomes manifest in a weak shoulder (marked by an arrow), but also at finite field, where the single step develops via a 0.7-anomaly into a double step of width $g_{\rm eff}\mu_B B$. Fig. 2b↑ and Fig. 2b↓ show the calculated spin-resolved conductance for the same fields and interaction used in Fig. 2a. As expected, the conductance increases/decreases for the favoured/disfavoured (spin-up/spin-down) electrons. But unlike in the non-interacting case (not shown) the spin-down step is shifted much more strongly towards negative values of $\tilde{V}_c$ than the spin-up shift is shifted towards positive values of $\tilde{V}_c$. This can be explained as follows: Once a finite field breaks spin-symmetry, interactions push away spin-down electron out of the QPC's center, thereby depleting their density around the barriers top and consequently strongly reducing their probability of transmission. The 0.7-anomaly at finite magnetic field is a natural consequence of this interaction-induced asymmetry.

As explained in detail in reference [9], the origin of the 0.7-anomaly is caused by the presence in the LDOS of the van Hove ridge. Its apex crosses the chemical potential, when the QPC is tuned into the sub-open regime, that is, when the for conductance takes values

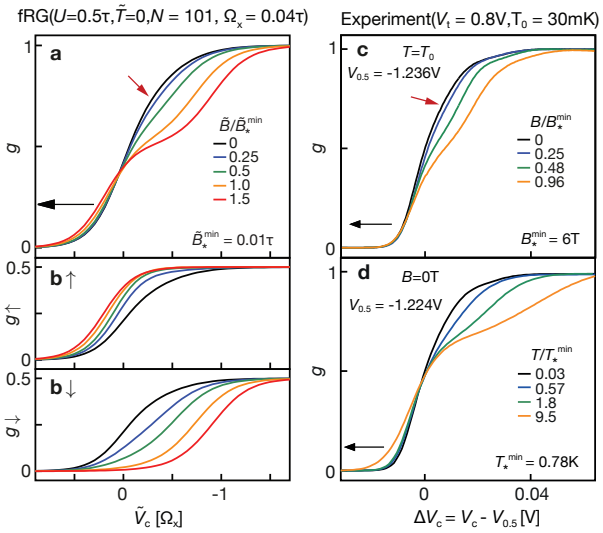

Figure 2 **a/c**, Calculated/measured linear conductance $g(V_c)$ as a function of barrier height/gate voltage for several values of magnetic field, at zero/low temperature we find good qualitative agreement: interactions cause a weak shoulder even at zero field, which strengthens for intermediate fields and eventually develops into a spin-resolved conductance step at high field. **b**↑/**b**↓, Calculated spin-resolved conductance curves for the same magnetic fields as in **a**. The conductance curves for spin-up and spin-down react in an asymmetric fashion on an applied field: a combination of Pauli exclusion principle and Coulomb blockade (Hartree effect) leads to a strong reduction of ↓-conductance, resulting in the phenomenon of the 0.7-anomaly. **d**, Measured conductance for several temperatures at zero field: The 0.7-anomaly gets more pronounced with temperature, while all other features are smeared out by thermal fluctuations.

$0.5 \lesssim g \lesssim 1$. As a consequence, the local spin-susceptibility, $\chi_j = \frac{1}{2}(\partial_h m)_{h=0}$, shows not only a strong j-dependence due to the inhomogeneity of the QPC, but also a strong $\tilde{V}_c$-dependence, when the potential is shifted through μ (see Fig. 3a). This also manifests itself in the total spin-susceptibility of the QPC, $\chi_{\rm tot} = \sum_{j\in \rm QPC} \chi_j$, which is plotted in Fig. 3b for several values of interaction strength. Three direct consequences of interactions stand out: First, interactions strongly enhance the effect of an applied magnetic field. Second, the maximum in the QPC's susceptibility is shifted to somewhat lower values of $\tilde{V}_c$ and, third, this maximum occurs when the QPC is sub-open (gray dashed vertical line in Fig.3, compare with conductance curves in Fig. 3c). These anomalous spatial structures in the spin susceptibility serve as the main incentive for the experimental work described further below, whose ultimate goal is to detect these structures by optical means.

Copyright line will be provided by the publisher

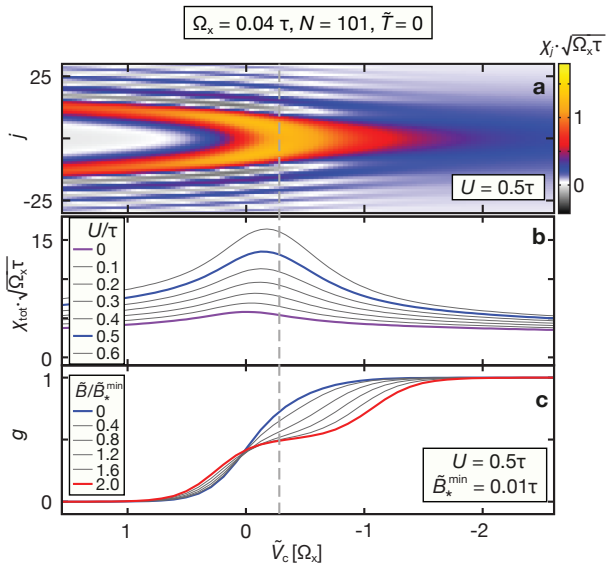

Figure 3 **a**, Local spin susceptibility, $\chi_j(\tilde{V}_c)$, as a function of site index j and barrier height $\tilde{V}_c$ for a fixed value of interaction strength, $U = 0.5\tau$. **b**, The total spin-susceptibility of the QPC, $\chi_{tot} = \sum_j \chi_j$ for several values of interaction strength. **a**. **c**, Calculated conductance curves as a function of barrier height for several values of magnetic field. The strongest response of the system to a small applied magnetic field happens in the center of the barrier (see **a**) and coincides with the barrier height for which the 0.7-anomaly occurs (highlighted with the gray dashed vertical line around $\tilde{V}_c = -0.25\Omega_x$).

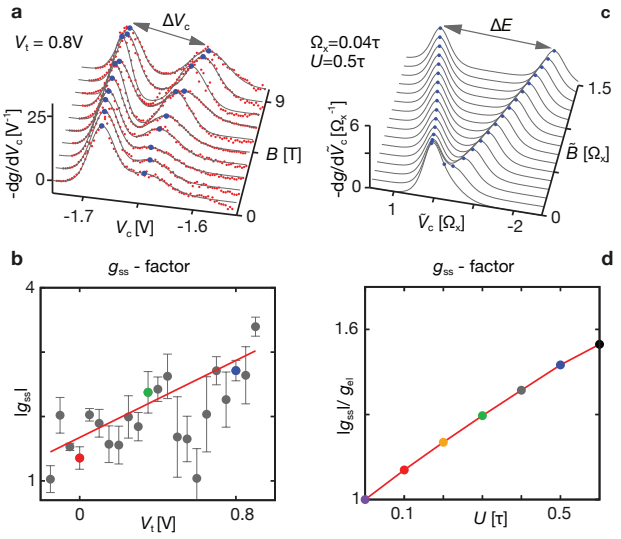

Figure 4 **a/c**, Measured/calculated transconductance, dg/dV_c, at fixed top gate/ interaction strength for several values of magnetic field. **b**,**d** Extracted values of the spin-splitting g-factor g_{ss} for several values of the top gate/interaction strength. The experiment confirms the theoretical prediction that increasing interaction strength also increases the value of g_{ss}.

Finally, we extracted the spin-splitting g-factor, $g_{\rm ss} = \frac{d\Delta E}{dB}$, for several values of top gate voltage, $V_{\rm t}$. Here ΔE depends on magnetic field and is the energetic difference between spin-up and spin-down modes. It can be extracted from the position of the maxima in the transconductance, $\frac{dg}{dV_c}$, as a function of gate voltage, V_c, (see Fig. 4a/c), together with an appropriate conversion factor $\Delta V_c = a\Delta E$. When varying the voltage of the top gate we find a clear trend, namely that increasing $V_{\rm t}$ increases $g_{\rm ss}$ as well (see Fig. 4b). This can be explained as follows: The top gate in effect tunes the channel width; the more positive its voltage the narrower the channel is, which in turn increases the effective interaction in the QPC. The prediction that increased interaction strength causes a larger $g_{\rm ss}$ is confirmed by our theoretical calculations, which reproduce the experimental trends quite beautifully (see Fig. 4c and Fig. 4d).

3 Theoretical motivation of the experiment Next, we describe ongoing experimental work, whose ultimate goal is to test the following prediction emerging from the theoretical work described above: For a QPC tuned in the regime of the 0.7-anomaly at zero external magnetic field theory predicts an enhancement in the local electron spin susceptibility [9]. At finite magnetic fields the enhanced spin susceptibility should give rise to electron-spin polarization with a spatial distribution characteristic of a QPC operated at the point of the 0.7-anomaly (see figure 3a). Moreover, this polarization would also result in spin-sensitive conductance. In principle, both signatures could be probed by optical means: while spatially-resolved Kerr or Faraday rotation could be used to map out the local spin-polarization in the vicinity of the QPC, polarization-selective optical spin-injection could be exploited to create an electron-spin imbalance across the QPC to drive spin-polarized currents.

Our first step en-route to combined transport and optical spectroscopy of a QPC in the 0.7-anomaly regime was to design a heterostructure that would allow to implement both spin-sensitive Faraday rotation and spin-selective charge carrier injection.

The following experimental part is divided into three sections. In Section 3.1 we discuss the optimization process of the heterostructure design and the results of the simulations performed with *nextnano3* [14]. In section 3.2 we present initial transport and optical characterization measurements of the heterostructure. Section 3.3 describes the present stage of our experiments and provides perspectives

Copyright line will be provided by the publisher

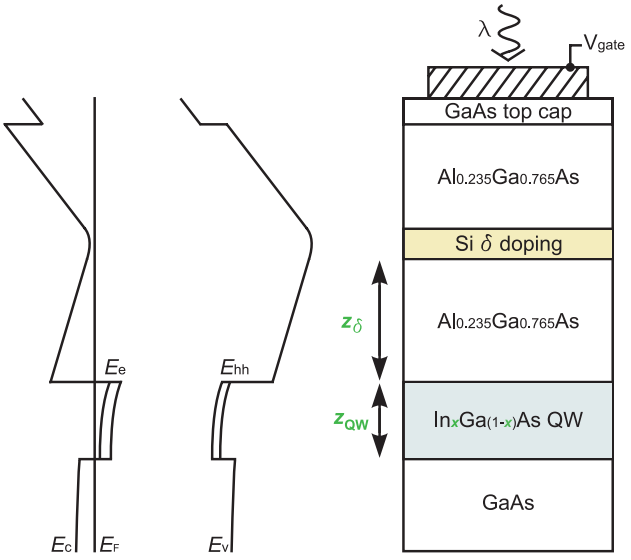

Figure 5 Right: Schematic design of the heterostructure. A 2DES is obtained in the InGaAs quantum well (blue) grown on top of GaAs by electron transfer from the delta-doping region (yellow) within the AlGaAs layer. A GaAs layer top cap layer terminates the heterostructure. A semi-transparent metal gate on top of the heterostructure gives rise to a built-in Schottky potential and allows to further bend the band structure via a voltage $V_{\rm gate}$. The quantum well thickness z_{QW}, the indium concentration x and the distance z_δ from the quantum well and the delta-doping region were used as optimization parameters in simulations with *nextnano3*. Left: Band structure profile along the growth direction obtained from simulations for $V_{\rm gate} = 0$. $E_{\rm c}$ and $E_{\rm v}$ denote the conduction and valance band edges, $E_{\rm e}$ and $E_{\rm hh}$ the lowest electron and heavy-hole levels confined in the quantum well, and $E_{\rm F}$ is the Fermi energy, respectively.

for the combined transport and optical spectroscopy of the 0.7-anomaly in a QPC.

3.1 Semiconductor heterostructure design and simulations The design of the heterostructure for combined transport and optical experiments was guided by two main objectives. On the one hand, we intended to realize a high quality two-dimensional electron system (2DES) suited for the observation of the 0.7-anomaly in a QPC. On the other hand the sample structure should be designed to allow for spin-selective optical excitations of charge carriers from the valence band into the conduction band states of the 2DES just above the Fermi level, and at the same time avoid excitations of charge carriers in any other heterostructure layer. To make all sample regions but the 2DES transparent to light at optical frequencies that meet the resonance condition for interband excitation of electrons into the Fermi sea we chose to embed an $\rm In_{\it x}Ga_{(1-\it x)}As$ quantum well (QW) hosting the 2DES in higher bandgap materials such as GaAs and AlGaAs. Accordingly, optical excitations from the valence band states into the conduction band states within the $\rm In_{\it x}Ga_{(1-\it x)}As$ QW exhibit the smallest energy for interband transitions, provided that the concentration x of indium is finite. At the same time quantum confinement associated with the QW removes the degeneracy of heavy- and light-hole subbands at the Γ-point of bulk zinc blende semiconductors, which in turn ensures "clean" dipolar selection rules for spin-selective optical excitations from the heavy hole subband at $E_{\rm hh}$ into the states at $E_{\rm F}$ of the 2DES.

Fig. 5 illustrates the basic layout of our heterostructure. The corresponding layer sequence along the sample growth direction is shown in the right panel of Fig. 5. The $\rm In_{\it x}Ga_{(1-\it x)}As$ QW of variable thickness z_{QW} and an indium fraction x in the range of $0 < x < 0.1$ is sandwiched between GaAs and $\rm Al_{0.235}Ga_{0.765}As$ that contains a delta-doping region located at a distance z_δ above the QW. The AlGaAs layer acts as a tunnelling barrier between the 2DES and the semitransparent Schottky gate deposited on top of the heterostructure. The overall thickness of the AlGaAs barrier was set to half of the wavelength of the expected QW interband transition to minimize optical interference effects. The silicon delta-doping provides for excess electrons to form a 2DES inside the QW and the final GaAs top cap layer prevents oxidization of the AlGaAs barrier. In the left panel of Fig. 5 the corresponding band structure profile calculated with *nextnano3* is shown for zero external gate voltage, $V_{\rm gate} = 0$, and $x = 0.07$, $z_{QW} = 10\rm nm$ and $z_\delta = 50\rm nm$. The band profile bending is due to the built-in Schottky potential, accounting for the lowest QW electron level $E_{\rm e}$ to lie below the Fermi energy, in accord with our intention to create a modulation-doped 2DES within the InGaAs QW.

We recall the main properties of the intended heterostructure. First the QW containing the 2DES should exhibit the smallest interband transition energy with well defined dipolar selection rules for spin-selective excitations. Second the semiconductor matrix above and below the QW should be transparent at the intended optical frequencies. Both criteria can be satisfied by the heterostructure layout of Fig. 1. Finally the density of the 2DES should be at least $2 \times 10^{11}\rm cm^{-2}$ to ensure the required transport characteristics.

To this end we used *nextnano3* to monitor the 2DES density as a function of the optimization parameters x, z_{QW} and z_δ. The objective was to achieve a maximum electron density inside the QW of about 3×10^{11} $\rm cm^{-2}$. Simultaneously the interband transition wavelength of the QW region, which follows from the energy difference between the lowest QW hole level and the Fermi energy, was intended to lie above 830 $\rm nm$ in order to not overlap with optical transitions of carbon impurities inherent to the molecular beam epitaxy (MBE) growth process of the heterostructure. In Fig. 5 these adjustable parameters for the simulations are highlighted in green. Raising the QW thickness $z_{\rm QW}$ as well as the QW indium content x mainly

Copyright line will be provided by the publisher

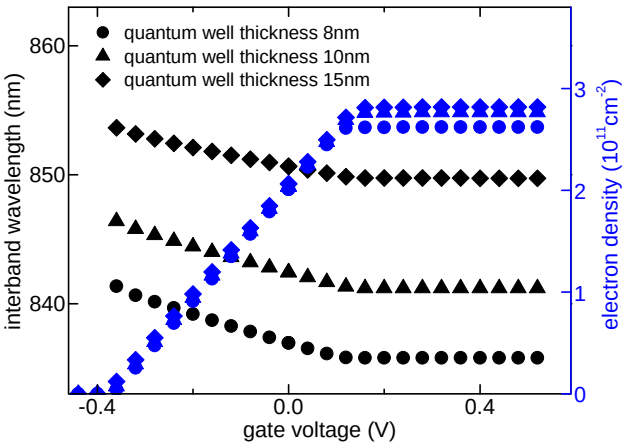

Figure 6 Simulation results for the QW electron density (blue) and the interband transition wavelength (black) as a function of gate voltage. Results are shown for three different QW thicknesses of $z_{\mathrm{QW}} = 8$ nm (circles), 10 nm (triangles) and 15 nm (squares) for a fixed indium content of $x = 0.07$ and a fixed spacer distance between the doping region and the QW of $z_\delta = 50$ nm.

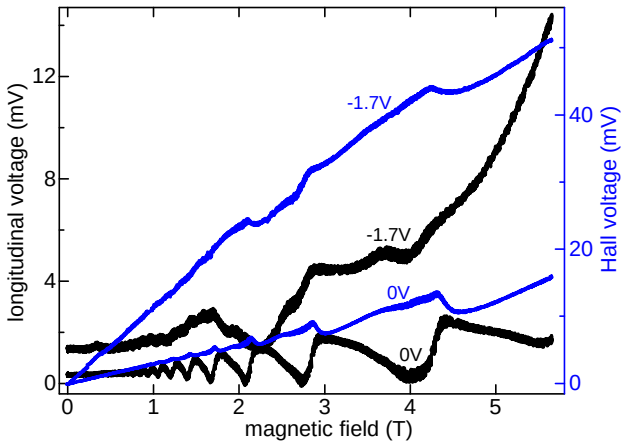

Figure 7 Measured longitudinal (black) and Hall voltages (blue) as a function of the perpendicularly applied magnetic field at topgate voltages of 0V and -1.7V.

increases the QW interband transition wavelength. Reducing the distance z_δ between the QW and the δ-doping layer tends to increase the 2DES density. However, at small QW thickness, proximity of the QW 2DES and the doping layer, and a high indium concentration typically reduce the mobility of the QW electrons and should be avoided.

Fig. 6 shows the simulation results for three different heterostructures with an indium concentration of $x = 0.07$ and $z_{\mathrm{QW}} = 50$ nm. The QW thickness was taken as 8 nm, 10 nm and 15 nm to obtain a variation in the QW electron density (blue) and the interband transition wavelength (black) as a function of the voltage applied to the semitransparent top gate. Decreasing the gate voltage increases the energy of the QW electron levels with respect to the Fermi energy which gradually depletes the 2DES density inside the QW. This depletion becomes increasingly pronounced below gate voltages of 0.15 V until the pinch-off is reached at about -0.4 V for all three heterostructures. The interband wavelength remains constant for $V_{\mathrm{gate}} > 0.25$ V. At more negative gate voltages the simulations predict a redshift of the resonance condition that is associated with a decrease of the Fermi energy. In Fig. 6 the maximum 2DES density as well as the optical transition wavelength are close to our intended values.

3.2 Basic transport and optical characteristics

Based on these simulation results a heterostructure was grown by MBE with an indium concentration of $x = 0.07$, the separation between the QW and the delta-doping layer of $z_{\mathrm{QW}} = 50$ nm, and a QW thickness of 10 nm (compare Fig. 5). Subsequently the sample material was characterized with respect to basic transport and optical properties. To determine the electron density and mobility of the 2DES a standard Hall bar geometry was used. The Hall bar mesa was fabricated by conventional wet etching techniques and AuGe/Ni/AuGe ohmic contacts were defined as Ohmic contacts to the 2DES. To allow control of the electron density a semitransparent titanium gate with a thickness of 5 nm was deposited on top of the central region of the Hall bar structure.

The electron density and mobility were extracted from four-terminal dc Hall voltage measurements before the sample was subjected to light. Magnetic fields of up to 5.7 T were applied perpendicularly to the QW plane. By fitting the Hall voltage U_{xy} versus the applied magnetic field B in the linear regime at low B (Fig. 7) the carrier density of the 2DES is extracted by

$$n_{\mathrm{2DES}} = \frac{I}{e \cdot dU_{\mathrm{xy}}/dB}. \qquad (2)$$

e is the elementary charge and I is the current through the Hall bar. The mobility μ_{2DES} of the electron system inside the QW was obtained from the longitudinal voltage at zero magnetic field $U_{\mathrm{xx}}(B = 0)$ (Fig. 7) using the relation

$$\mu_{\mathrm{2DES}} = \frac{0.75}{e \cdot n_{\mathrm{2DES}} \cdot U_{\mathrm{xx}}(B = 0)} \qquad (3)$$

and the electron density n_{2DES} obtained according to Eq. (2). The number in the numerator is a scaling factor imposed by the particular geometry of the employed Hall bar structure. The same procedure was also carried out after broad-band illumination of the sample.

In a second step we studied basic optical properties of the sample by investigating the photoluminescence (PL) from the Hall bar. A cryogenic confocal microscope with an optical spot size of 1 μm was used to record the local PL response, which was then spectrally dispersed by a monochromator and detected with a low-noise liquid nitro-

Copyright line will be provided by the publisher

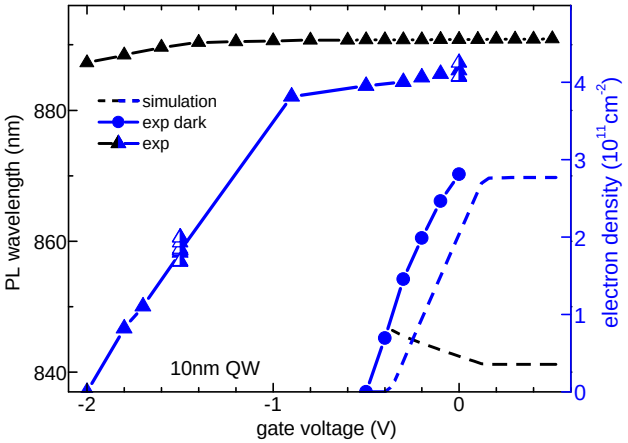

Figure 8 Transport and optical characterization of the heterostructure. Data (symbols; lines are guides to the eye) and corresponding simulations as in Fig. 6 (dashed lines) for a heterostructure with a QW of thickness $z_{\mathrm{QW}} = 10\ \mathrm{nm}$, 7% of indium concentration, and $z_\delta = 50\ \mathrm{nm}$. The wavelength of the photoluminescence peak maximum and the electron density of the QW 2DES are shown as a function of gate voltage in black and blue, respectively. Circles and triangles indicate the measurement results before and after light illumination of the Hall bar, respectively. Half-filled triangles correspond to electron densities measured after repeated illumination of the sample. The photoluminescence was obtained from the central region of the Hall bar using a confocal setup with excitation powers of 7 μW in the range of $+0.6$V to -1.0V and 0.3 μW below -1.0V at an excitation wavelength of 830 nm. The 2DES density was derived from standard Hall measurements. All measurements were carried out at 4.2 K.

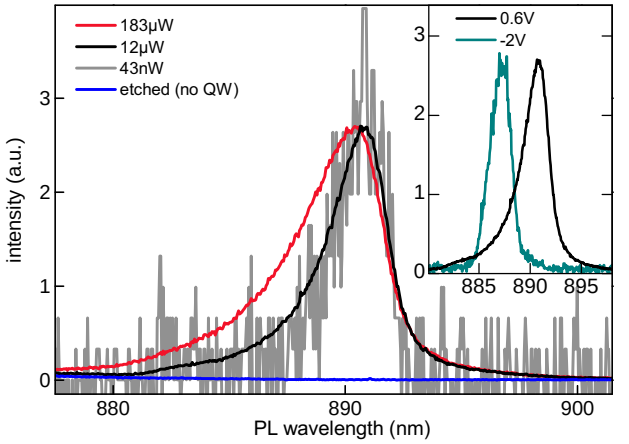

Figure 9 Photoluminescence spectra recorded for a Hall bar sample at 4.2K with a QW thickness of 10 nm and incident excitation powers of $P_{\mathrm{exc}} = 183\ \mu$W (red), 12 μW (black, main and inset graph) and 43 nW (grey) scaled to maximum intensity values. The photoluminescence spectra were measured in the central Hall bar region at gate voltages of $V_{\mathrm{gate}} = +0.6$ V (flatband) under cw excitation at a wavelength of 830 nm. The photoluminescence from an area where the QW was etched away is shown in blue for reference. Inset: photoluminescence spectra at two different gate voltages of $+0.6$ V (black) and -2.0 V (green) for incident excitation power of 300 nW.

gen cooled CCD. All measurements were carried out at a sample temperature of 4.2 K.

The combined transport and optical characterization results are shown in Fig. 8. The interband transition wavelength (black) and the QW electron density (blue) are shown as a function of gate voltage. Circles (triangles) indicate the results of measurements done before (after) illumination of the the sample with continuous wave (cw) lasers (with 815 nm and 830 nm center wavelength). Dashed lines show the corresponding simulation results from Fig. 6 for comparison. In the simulations all silicon dopants were assumed to be ionized, which is realized experimentally by sample illumination. Despite an increase by $\sim 30\%$ of the 2DES density to around $4.2 \times 10^{11}\mathrm{cm}^{-2}$, upon illumination, the simulated and experimental results are in very good agreement with the predictions of the simulation. Consistently, the pinch-off gate voltage where the carrier density goes to zero is shifted to more negative values upon illumination compared to the simulated pinch-off voltage. Repeated illumination of the sample did not introduce further significant changes in the 2DES density (half-filled triangles in Fig. 8), indicating a long-term stability of the 2DES density after the initial ionization of silicon dopants. The mobility of the 2DES was determined to $\sim$ 70000 cm^2/Vs within the entire gate voltage range above -1.5V after sample illumination (data not shown).

Despite good agreement between simulations and experiment for the 2DES density, we found considerable discrepancy between expected and observed values for the wavelength of the optical transition that we monitored via PL. Fig. 8 shows the wavelength of the PL peak as a function of gate voltage recorded near the center of the Hall bar. Incident laser excitation powers were 7 μW in the voltage range between $+0.6$ V and -1.0 V and 0.3 μW below -1.0 V, respectively. The excitation wavelength was set to 830 nm, close to the wavelength region of carbon impurity states in GaAs at 4.2 K. The mean difference between the simulated and the measured optical transition wavelength is about 50 nm featuring different signs of the optical resonance shift. We speculate that the discrepancy partially arises from excitonic effects and the quantum confined Stark effect that were not accounted for in our simulations. Nevertheless, our main objective of the heterostructure design aiming at optical QW transition energies below the band gap of GaAs was successfully achieved.

Fig. 9 shows the spectral characteristics of the PL. The spectra were measured with a confocal setup in the central Hall bar region at gate voltages of $+0.6$ V (flatband con-

Copyright line will be provided by the publisher

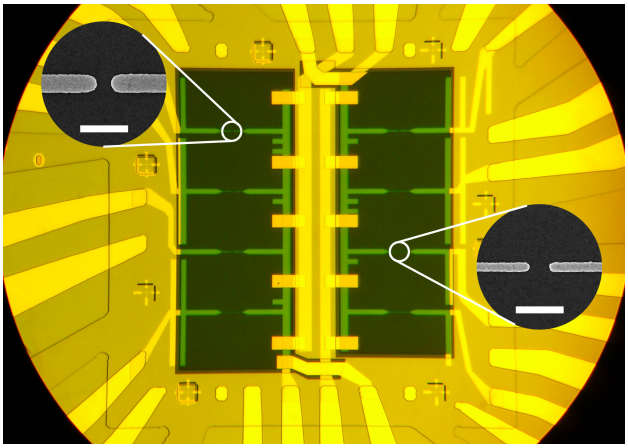

Figure 10 Optical microscope image of the sample layout with eight QPCs and a global top gate fabricated on the $10\ \mathrm{nm}$ InGaAs QW heterostructure. Optical and electron-beam lithography followed by gold deposition and lift-off were used to define gates on top of a square mesa with an edge length of $160\ \mu\mathrm{m}$. The QPCs are formed between the ends of finger-like gates (also shown as scanning-electron micrograph insets each including a horizontal scale bar corresponding to $1\mu\mathrm{m}$ length) of different geometries. On the top of the mesa a semitransparent gate was deposited that is electrically disconnected by cross-linked PMMA from all other gates used to define the QPCs.

dition) for a cw laser excitation wavelength of $830\ \mathrm{nm}$ at $4.2K$. The PL exhibits an asymmetric profile reminiscent of Fermi edge singularity [15,16,17] even at lowest excitation powers down to $\sim 40\ \mathrm{nW}$ (grey spectrum in Fig. 9). Unambiguously, the source of the PL is the QW, since no PL was detected in the relevant spectral window from sample regions were the QW was etched away (blue spectrum in Fig. 9). We find indications of higher-energy shoulders at $883\ \mathrm{nm}$ and $885\ \mathrm{nm}$ that emerge with increasing excitation powers accompanied by a blue-shift of the PL maximum. These characteristics were consistently found at different spatial locations of the Hall bar structure were the QW was not etched away. We also found that the PL was sensitive to the gate voltage. The inset of Fig. 9 compares the PL spectra at $V_{\mathrm{gate}} = +0.6\ \mathrm{V}$ and $-2.0\ \mathrm{V}$, showing a clear blue-shift of the PL resonance with more negative gates voltages that was accompanied by a gradual evolution of the PL line shape towards a symmetric Gaussian peak (fit not shown).

3.3 Outlook The basic properties of the heterostructure described above represent a promising starting point for in-detail transport and optical studies of the 0.7-anomaly in QPCs. Fig. 10 shows an optical micrograph of our present sample layout implemented on a heterostructure that contains a 2DES hosted by an InGaAs QW of $10\ \mathrm{nm}$ thickness. Gold gates defined by optical lithography (outer yellow pads) connect to inner Au gates processed by electron beam lithography (light yellow) across the mesa-edges (centered square and starlike surrounding connections). Eight QPCs of different widths and lengths of the gated constrictions between $200\mathrm{nm}$ and $500\mathrm{nm}$ are covered by layers of cross-linked Poly Methyl methacrylate (PMMA) (dark grey). The latter electrically isolates the QPC gates from the two semitransparent Nickel-Chromium top gates of $5\mathrm{nm}$ thickness (black rectangles on top of the PMMA in Fig. 10). They allow to simultaneously having optical access to the 2DES layer and being able to tune its carrier density. The insets in Fig. 10 show SEM pictures of two specific QPC geometries.

The next step will involve transport experiments to study the 0.7-anomaly as a function of the QPC geometries in the accessible experimental parameter space. In opto-transport experiments we will then attempt to optically monitor the field-dependence of the spin-up and spin-down densities in the vicinity of the QPC as a function of QPC gate voltage V_{c} and top gate voltage V_{t}. We will also aim to perform near-resonant injection of spin-polarized electrons in the vicinity of a QPC to observe spin-selective transport. We intend to exploit the full potential of the combined optical and transport setup in terms of position, energy and spin selective spectroscopy to shed light on the microscopic origin of the 0.7-anomaly.

Acknowledgements We acknowledge discussions with J. P. Kotthaus. We gratefully acknowledge funding by the Deutsche Forschungsgemeinschaft within the priority program "Semiconductor Spintronics" (SPP 1285) and the center of Excellence, Nanosystems Initiative Munich (NIM), and financial support from the Center for NanoScience (CeNS).

References

[1] B. J. van Wees, H. van Houten, C. W. J. Beenakker, J. G. Williamson, L. P. Kouwenhoven, D. van der Marel, C. T. Foxon, Phys. Rev. Lett., **60**, 848 (1988)
[2] D. A. Wharam, T. J. Thornton, R. Newbury, M. Pepper, H. Ahmed,J. E. F. Frost, D. G. Hasko, D. C. Peacock, D. A. Ritchie and G. A. C. Jones, J. Phys. C, **21**, L209 (1988)
[3] M. Büttiker, Phys. Rev. B, **41**, 7906 (1990)
[4] K. J. Thomas, J. T. Nicholls, M. Y. Simmons, M. Pepper, D. R. Mace and D. A. Ritchie, Phys. Rev. Lett., **77**, 135 (1996)
[5] K. J. Thomas, J. T. Nicholls, N. J. Appleyard, M. Y. Simmons, M. Pepper, D. R. Mace, W. R. Tribe and D. A. Ritchie, Phys. Rev. B, **58**, 4846 (1998)
[6] N. J. Appleyard, J. T. Nicholls, M. Pepper, W. R. Tribe, M. Y. Simmons, D. A. Ritchie, Phys. Rev. B, **62**, R16275 (2000)
[7] S. M. Cronenwett, H. J. Lynch, D. Goldhaber-Gordon, L. P. Kouwenhoven, C. M. Marcus, K. Hirose, N. S. Wingreen and V. Umansky, Phys. Rev. Lett., **88**, 226805 (2002)
[8] A. P. Micolich, J. Phys. Condens. Matter, **23**, 443201 (2011)
[9] F. Bauer, J. Heyder, E. Schubert, D. Borowsky, D. Taubert, B. Bruognolo, D. Schuh, W. Wegscheider, J. von Delft and S. Ludwig, Nature, **501**, 73 (2013)

Copyright line will be provided by the publisher

[10] C. Wetterich, Phys. Lett. B, **301**, 90 (1993)
[11] W. Metzner, M. Salmhofer, C. Honerkamp, V. Meden and K. Schönhammer, Rev. Mod. Phys., **84**, 299 (2012)
[12] V. Meden, W. Metzner, U. Schollwöck and K. Schönhammer, Phys. Rev. B, **65**, 045318 (2002)
[13] S. Andergassen, T. Enss, V. Meden, W. Metzner, U. Schollwöck and K. Schönhammer, Phys. Rev. B, **70**, 075102 (2004)
[14] http://www.nextnano.de/nextnano3
[15] G. D. Mahan, Phys. Rev., **153**, 882 (1967)
[16] P. Hawrylak, Phys. Rev. B, **44**, 3821 (1991)
[17] C. L. Kane, K. A. Matveev and L. I. Glazman, Phys. Rev. B, **49**, 2253 (1994)

Copyright line will be provided by the publisher